Cellular Microbiology (2007) **9**(2), 413–424

doi:10.1111/j.1462-5822.2006.00799.x
First published online 31 August 2006

Real-time studies of the progression of bacterial infections and immediate tissue responses in live animals

Lisa E. Månsson,[1] Keira Melican,[1] Jorrit Boekel,[1] Ruben M. Sandoval,[2] Isabelle Hautefort,[3] George A. Tanner,[4] Bruce A. Molitoris[2] and Agneta Richter-Dahlfors[1]*

[1]*Department of Microbiology, Tumor and Cell Biology, Karolinska Institutet, S-171 77 Stockholm, Sweden.*
[2]*Division of Nephrology, Department of Medicine, Indiana Center for Biological Microscopy, Indianapolis, IN 46202, USA.*
[3]*Pathogen Molecular Microbiology, Institute of Food Research, Norwich NR4 7UA UK.*
[4]*Department of Cellular and Integrative Physiology, Indiana University School of Medicine, Indianapolis, IN 46202, USA.*

Summary

By combining intravital multiphoton microscopy and bacterial genetics we have developed a technique enabling real-time imaging of bacterial proliferation and tissue responses in a live animal. Spatial and temporal control of the infection process was achieved by microinjecting GFP$^+$-expressing uropathogenic *Escherichia coli* (UPEC) into tubules of exteriorized kidneys in live rats. GFP$^+$ was introduced in the clinical UPEC strain CFT073 as a single-copy chromosomal gene fusion. Within hours, bacterial colonization was accompanied by marked ischaemic effects, perivascular leakage, loss of tubular integrity and localized recruitment of immune cells. The pathophysiology was altered in response to an isogenic bacterial strain lacking the exotoxin haemolysin, revealing the subtle and temporal roles of bacterial virulence factors *in vivo*. Microdissection and RNA extraction of the injected nephron allowed molecular analysis of prokaryotic and eukaryotic gene expression. The techniques described here can be applied to study the integrated cell communication evoked by a variety of bacterial pathogens, assisting in the design of strategies to combat bacterial infections.

Received 9 June, 2006; revised 11 July, 2006; accepted 12 July, 2006. *For correspondence. E-mail agneta.richter.dahlfors@ki.se; Tel. (+46) 8 5248 7425; Fax (+46) 8 34 26 51.

Introduction

The inflammatory response triggered by microbial infections is often accompanied by a dramatic alteration in tissue homeostasis. A dynamic and fine-tuned response to infection is crucial to avoid unnecessary tissue damage or conditions such as chronic inflammation and cancer (Lax and Thomas, 2002; Karin and Greten, 2005). Previous research in bacterial pathogenesis has focused on bacteria-induced signals in individual cells, the main challenge of current research is to understand how these signals are transduced from the primary target to induce a synchronized tissue response. Unfortunately the availability of techniques for studying the continuity of infection within a single animal is limited.

Multiphoton microscopy is a non-invasive technique providing resolution at cell level. It has successfully been applied to intravital physiological organ studies (Dunn *et al*., 2003), tumour biology (Brown *et al*., 2001) and embryonic development (Squirrell *et al*., 1999). As multiphoton imaging permits real-time collection of optical sections deep into organs of live animals, studies can be performed with the full complement of influencing vasculature, nerves and extracellular matrix intact (Dunn *et al*., 2003). The difficulty in achieving stable fluorescent labelling of bacteria *in vivo* has previously prevented the application of this technique to microbial pathogenesis. Plasmid-borne expression of autofluorescent proteins, such as green fluorescent protein (GFP), requires selection pressure for plasmid maintenance. This can be difficult to achieve inside an animal during the time course of infection, often spanning several days. Variation of plasmid copy numbers can cause quantification problems as well as toxic levels of GFP (Hautefort *et al*., 2003). The migration of bacteria through changing microenvironments inside an animal puts specific constraints on the choice of promoter for efficient GFP expression at various phases of infection.

Pyelonephritis represents an infectious condition where bacteria pass through a variety of microenvironments as they spread from the tubular lumen of the infected nephron into deeper tissues. This is accompanied with an acute inflammatory response leading to massive tissue destruction particularly in the cortical parenchyma

Table 1. *Escherichia coli* strains and oligonucleotides.

Strain	*Genotypes and serotypes*	*Reference*
CFT073	O6:K2:H1	Mobley *et al*. (1990); Welch *et al*. (2002)
LT002	CFT073 *hlyA::km*^{r}	This study
LT003	CFT073 *cobS::gfp*+, *cm*^{r}	This study
LT004	CFT073 *cobS::*ϕ(*P*$_{LtetO-1}$-*gfp*$^+$), *cm*^{r}	This study
LT005	LT002 *cobS::*ϕ(*P*$_{LtetO-1}$-*gfp*$^+$), *cm*^{r}, *km*^{r}	This study
Oligonucleotide	*Sequence*	
P1hly[a]	atctttgcaccacaattagacaaattactgcaaaagtatTGTGTAGGCTGGAGCTGCTTC	
P2hly[a]	actgccaaaaaacttgtcggcacgcgtggtcccaataagCATATGAATATCCTCCTTAG	
P1cob[b]	gtgacgggaggcgcacggagcgggaagagtcgccacgcaGCCTGGGGTAATGACTCTCTAGC	
P2cob[b]	cagcgtatcgcccgtttgcccgcccagcgtacgtttgagaCGTCATTTCTGCCATTCATCC	
Ptet_F1[c]	CATGCGACCCGGGTTCGTCTTCACCTCGAGTCC	
Ptet_R1[c]	GTCGCCATTCTAGACCCATGGGTACCTTTCTCCT	
GAPDH_F	CACCACCAACTGCTTAGCC	
GAPDH_R	GGATGCAGGGATGATGTTCT	
CINC_F	**GCGGAGAGATGAGAGTCTGG**	
CINC_R	AGGCATTGTGCCCTACAAAC	
ICAM1_F	AGCATTTACCCCTCACCCAC	
ICAM1_R	CATTTTCTCCCAGGCATTCTC	
CD45_F	**AAGTCTTTGTCACAGGGCAA**	
CD45_R	TAACGCACAGTAACGTTCCC	
LFA1 α_F	GGGCAATGTCGACCTAGTGTTTCTG	
LFA1 α_R	GGCAAATATGTGGAGTTTCTCCTGC	
TNF α_F	TACTGAACTTCGGGGTGATCG	
TNF α_R	CCTTGTCCCTTGAAGAGAACC	
16S_F	CAGCCACACTGGAACTGAGA	
16S_R	ATTCCGATTAACGCTTGCAC	
Hly_F	GGGGATAATTTCAGGCATCC	
Hly_R	TCCCAATGTTGCTGGGTAAT	
P$_{LtetO-1}$[d,e]	*TTCGTCTTCACCTCGAG**TCC**CTATCAGTGATAGAGATTGACATCCCT*	
	ATCAGTGATAGAGATACTGAGCACATCAGCAGGACGCACTGACG	
	AATTCATTAAAGAGGAGAAAGGTACCCATGGG	

a. Lower case sequences are homologous to the *hlyA*-sequence on the CFT073 chromosome (bp 3419220-3419258 and bp 3421059-3421097 respectively).
b. Lower case sequences are homologous to the *cob*-sequence on the CFT073 chromosome (bp 2320640-2320602 and bp 2319418-2319457 respectively).
c. Underlined sequences indicate locations of restriction sites used for cloning.
d. Bold sequence encodes the tetracycline promoter. Italic sequence shows binding site of Ptet_R1 and Ptet_F1.
e. The $P_{LtetO-1}$ promoter is cloned from the pPROTet.E133 plasmid (BD Biosciences, CA, USA).
ϕ indicates transcriptional gene fusion.

(Heptinstall and Hill, 1983). The severity of infection is apparent, as pyelonephritis is a significant factor for development of renal scarring and end-stage renal failure in children. However, the pathophysiology of renal scarring is still unclear, which makes the prevention of renal damage difficult (Jahnukainen *et al*., 2005). As the pathologic outcome of the disease is influenced by early inflammatory events, a deeper understanding of the mechanisms of these early responses is of importance when exploring novel treatment options (Glauser *et al*., 1978; Shimamura, 1981).

Here we describe how a clinical uropathogenic *Escherichia coli* (UPEC) isolate, genetically modified to enable *in vivo* analysis, and multiphoton microscopy were used to obtain spatial and temporal resolution of the progression of infection in a rat model of pyelonephritis. Bacteria were injected directly into the lumen of superficial proximal tubules of exteriorized kidneys, enabling visualization of infection progression from the first interaction between pathogen and host. Multiphoton imaging followed by prokaryotic and eukaryotic gene expression analysis revealed novel cellular and molecular details of tissue responses during the first 24 h of infection. Despite extensive knowledge of the actions and signalling pathways triggered by bacterial virulence factors in cell lines (Philpott *et al*., 2001), their *in vivo* role remains unclear. Our studies revealed that the UPEC exotoxin haemolysin (Hly) altered the dynamics of the inflammatory response within the living organ.

Results

Generation of single-copy GFP$^+$ *gene fusions in clinical strains*

To enable *in vivo* detection of bacteria, a single-copy of a *gfp*$^+$-containing DNA fragment was inserted into the chromosomal *cobS* gene of the clinical UPEC isolate CFT073 under the control of the constitutively active tetracycline promoter $P_{LtetO-1}$, generating strain LT004 (Table 1). A

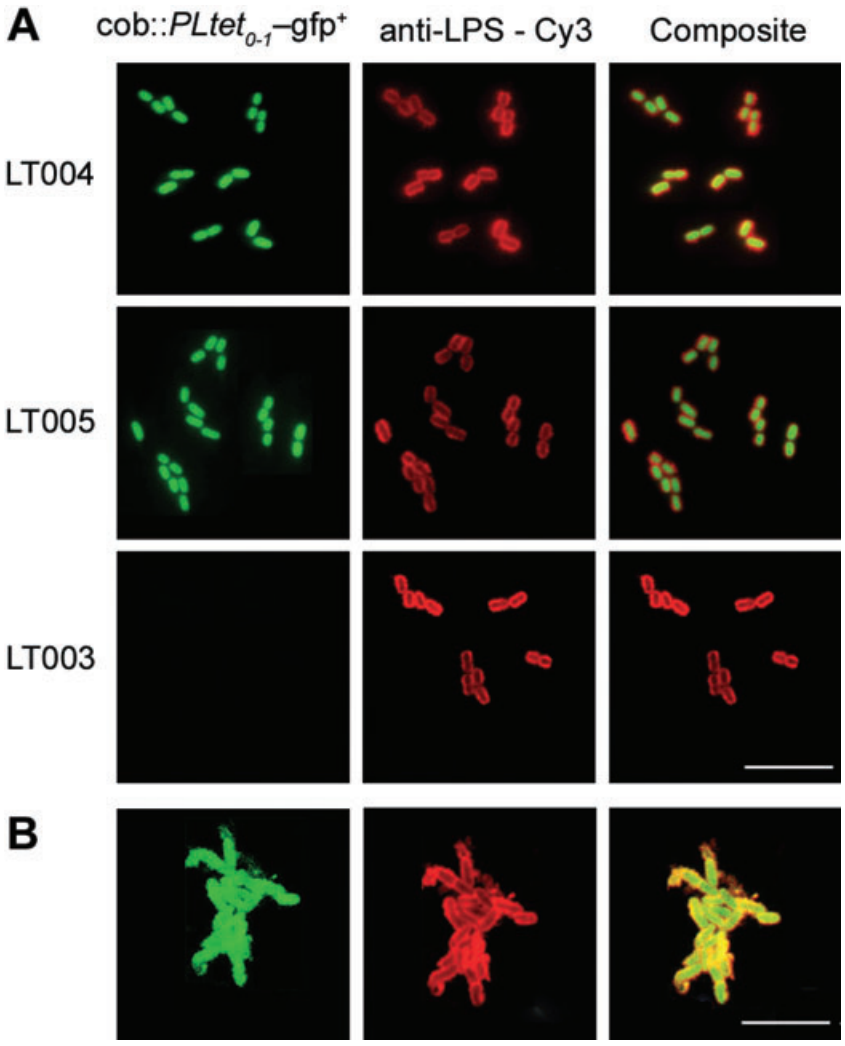

Fig. 1. Bacterial expression of GFP$^+$. Strains LT004 ($P_{LtetO-1}$-*gfp*$^+$-*cm*^{r}), LT005 ($P_{LtetO-1}$-*gfp*$^+$-*cm*^{r}, *hlyA::km*) and LT003 (promoterless *gfp*$^+$-*cm*^{r}) detected by immunohistochemistry using α-LPS and α-Cy3-antibodies (red) or endogenous GFP$^+$ expression (green). (A) *in vitro* and (B) *in vivo*. Scale bars represent 10 μm.

GFP$^+$-producing variant of CFT073 *hlyA*$^-$, LT005 and a control strain LT003, lacking the $P_{LtetO-1}$ promoter, were also constructed. Confocal microscopy confirmed stable, 100% expression of GFP$^+$ from LT004 and LT005 colabelled with anti-LPS–Cy3 antibodies (Fig. 1A). No expression was seen in strain LT003 (Fig. 1A). Strain LT004 [10^8 colony-forming units (cfu)] was used in a retrograde rat model of UTI (Uhlen *et al*., 2000) and showed 100% colocalization between GFP$^+$ expression and LPS in the kidney (Fig. 1B), verifying that the *cobS*::$P_{LtetO-1}$-*gfp*$^+$ gene fusion was suitable for bacterial detection *in vivo*.

Multiphoton microscopy for intravital analysis of ascending pyelonephritis

Following a four day retrograde pyelonephritis model of LT004, the rats were prepared for multiphoton imaging by carefully exteriorizing the kidney (Dunn *et al*., 2002) (Fig. 2A). In a PBS-injected control animal proximal tubules are discernible by their distinct shape and autofluorescence (punctuate dull green), while distal tubule cells lack this autofluorescence. The extensive vascularization of the kidney, allows for ready labelling of renal structures by intravenous injection of fluorescent probes via a femoral vein catheter. Injection of the DNA-binding probe Hoechst labelled the nuclei of individual tubule cells (blue), and the renal vasculature was labelled with tetramethyl rhodamine-conjugated 500 kDa dextran, a fluid phase marker retained in the vasculature (Fig. 2B). Erythrocytes in the blood stream exclude dextran, and are discernible as black streaks. Movie S1 shows the movement of erythrocytes through the blood vessels over a 40 s time period.

A four day retrograde LT004 infection induced large abscesses on the superficial cortex. Obstructed blood flow limited distribution of the red vascular dye and the nuclear stain, resulting in a dark area. Lack of autofluorescence demonstrated loss of tissue integrity in both *x*–*y* and *x*–*z* projections (Fig. 2C, upper and lower panels). Bacteria were rarely seen in necrotic tissue, but were

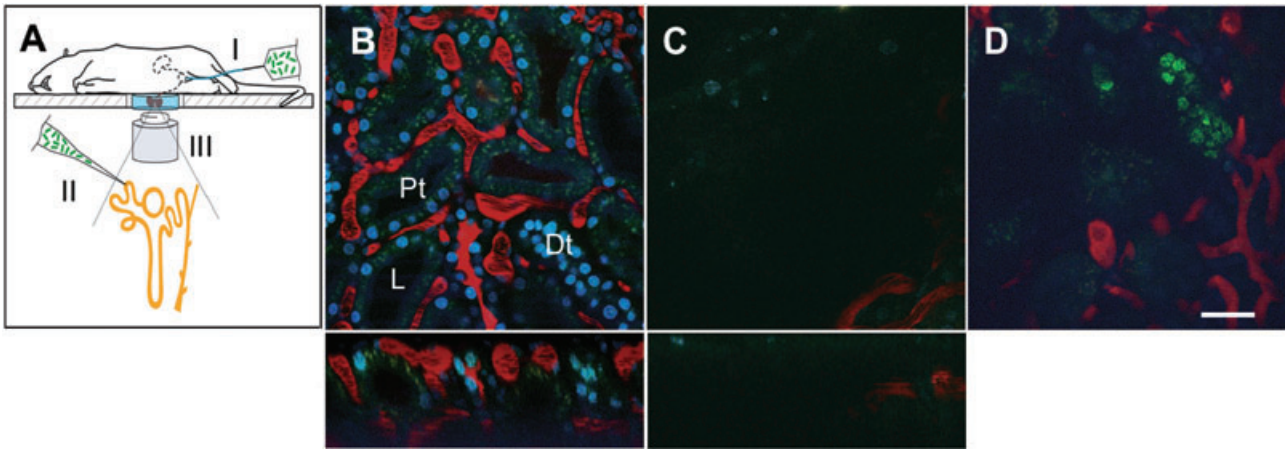

Fig. 2. Visualization of pyelonephritis by multiphoton microscopy.
A. Graphical depiction of experimental set-up. (I) Ascending retrograde infection where bacteria are infused into the bladder. (II) Bacteria injected by micropuncture directly into a proximal tubule of an exteriorized kidney. (III) Infection imaged by multiphoton microscopy.
B–D. Live kidney tissue morphology, where fluorescent 500 kDa dextran labels blood flow (red), cell nuclei are labelled with Hoechst stain (blue) and proximal tubules are identified by dull green auto-fluorescence.
B. An image originating from a 60-μm-thick volume collected from the superficial cortex of a sham-operated (PBS) control rat with proximal tubules (Pt), distal tubules (Dt) and tubular lumen (L) marked (upper panel). Lower panel shows the *x–z* projection.
C. Four days post infection with LT004 (*x–y* top panel, *x–z* lower panel).
D. A projection of an 18-μm-thick volume from the periphery of the infection site shown in (C). Scale bar represents 30 μm.

evident as distinct clusters on the periphery, suggestive of an intracellular location (Fig. 2D). Residual red fluorescence outlines an uncompromised subset of capillaries. Movie S2 shows an animation of this volume.

Live imaging of tissue remodelling during renal infection

A major limitation of the UTI retrograde model is the random ascension of bacteria into individual nephrons, preventing analysis of initial interactions between bacteria and host. To overcome this, we employed a micropuncture technique, injecting GFP$^+$-expressing *E. coli* (or PBS in sham-operated animals) directly into the lumen of superficial proximal tubules of exteriorized kidneys and subsequently visualizing the infection by multiphoton microscopy. LT004 were injected into the superficial proximal tubule lumens, along with Cascade blue-conjugated 10 kDa dextran and the dye Fast Green FCF, using micropipettes. Bacterial physiology was unaffected by these dyes. The coloured Fast Green FCF labelled the direction and speed of fluid flow during the injection process. Cascade blue-conjugated dextran accumulated rapidly in endosomes/lysosomes of proximal tubule cells, selectively outlining the injected tubule. Figure 3A shows several sections of the injected proximal tubule winding through the cortex 1 h post injection. Careful examination revealed individual, green bacteria attached to the tubular lining (Fig. 3A, arrows). Within hours, extensive bacterial multiplication resulted in massive luminal green fluorescence (Fig. 3B). Perturbed blood flow, depicted by a lack of red stain in the area adjacent to the infected tubule, highlighted the rapid effect of bacterial-induced mucosal signalling on the local circulation. Re-exteriorization of the kidney the following day revealed total disruption of the cortical tissue and efficient bacterial clearance (Fig. 3C). This rapid process was contained to the infected nephron, as intact tubular structures and normal capillary blood flow were observed in an adjacent, non-micropunctured nephron (Fig. 3D).

Addition *ex vivo* of Hoechst nuclear stain and an antibody directed towards CD18 identified recruited immune cells in the destructed area (Fig. 3E and F). Figure 3E shows the defined border between the normal morphology, identified by proximal tubular autofluorescence (left), and the inflamed area (right), where many recruited leukocytes exhibited segmented nuclei, characteristic of polymorphonuclear neutrophils (Fig. 3F). Some neutrophils contained engulfed bacteria (arrow) highlighting their efficiency pathogen removal.

Immediate local effects on the vasculature

To analyse the rapid development of pathology, the micropunctured tubule was observed every 30 min for 8 h. Figure 4A and B show two sites of an infected tubule with different luminal bacterial loads 4.5 h after microinjection of LT004. While some normal blood flow was still evident (Fig. 4A, I), effects such as plasma streaming, where capillaries are congested to such extent that erythrocytes cannot pass (Fig. 4A, II), and complete cessation of blood flow (Fig. 4A and B, III) were seen already at this early

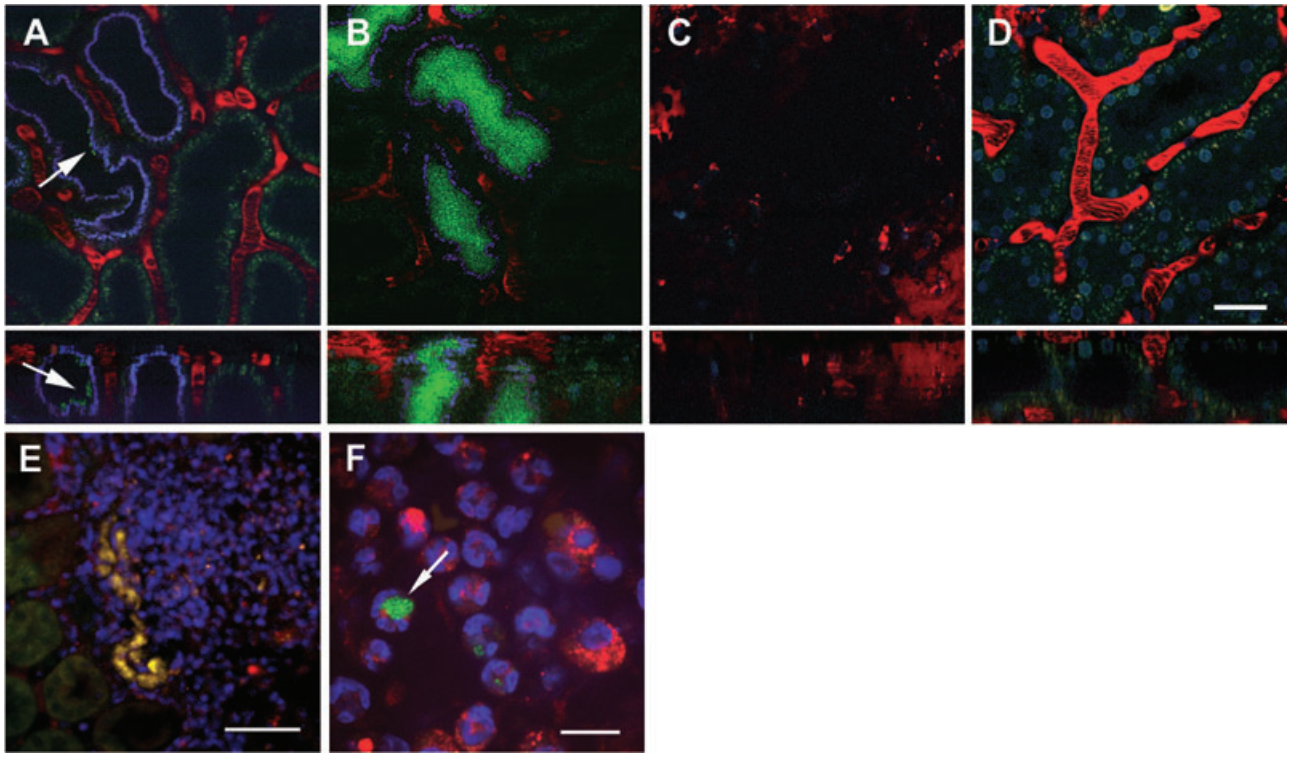

Fig. 3. Real-time imaging of LT004 infection. Ten kDa labelled dextran (blue) outlines the injected tubule, 500 kDa labelled dextran denotes blood flow (red in A–D), and bacteria are detected by GFP$^+$ (green).
A. A 50-μm-thick volume 1 h after injection (*x–y* top panel, *x–z* lower panel). Arrows indicate bacteria.
B. Five hours post injection.
C. A 65-μm-thick volume 22 h post injection.
D. Adjacent, non-infected, nephron of the same kidney after 22 h. Scale bar represents 30 μm.
E. The infected site in the kidney in C analysed by confocal microscopy *ex vivo*. Hoechst stain (blue) was added along with the leukocyte marker α-CD18-Cy3 (red). The 10 kDa dextran is pseudo-coloured yellow. Scale bar represents 50 μm.
F. Same site as in E, where neutrophils are identified by α-CD18-Cy3 (red) and distinct nuclear morphology (blue). Arrow indicates neutrophil phagocytosing bacteria. Scale bar represents 10 μm.

stage. These effects were accompanied by increased endothelial permeability, causing perivascular leakage of the large, red dextran (Fig. 4C, IV) in an area between the site of infection and the renal capsule. Extravasated immune cells, shown as black silhouettes within the leakage, were also observed (Fig. 4C). Adjacent, non-infected nephrons showed little signs of vascular dysfunction (Fig. 4D), highlighting the localization of these effects.

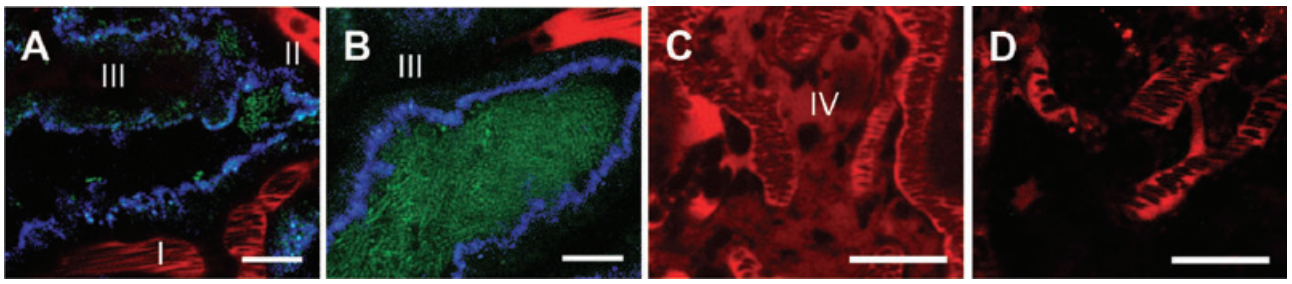

Fig. 4. Local vascular effects.
A–B. Two sections of a nephron 4.5 h post intratubular injection of LT004. Injected proximal tubule is outlined with 10 kDa labelled dextran (blue), blood flow is labelled by 500 kDa dextran (red), and bacteria are detected by GFP$^+$ (green). A (I) indicates normal blood flow, A (II) plasma streaming, while (III) in A and B points to occluded vessels.
C. Perivascular leakage below the renal capsule. (IV) indicates the presence of 500 kDa labelled dextran within the perivascular space.
D. Neighbouring, non-infected nephron. Scale bar represents 30 μm.

Instigation of immune response

Mucosal epithelial linings exposed to microbes rapidly release signalling molecules inducing a synchronized immune response spearheaded by the polymorphonuclear neutrophils (Pass and Freeth, 1993). The limited availability of intravital dyes restricted our ability to analyse recruitment and accumulation of leukocytes during live imaging. Rats imaged with multiphoton microscopy were therefore sacrificed after 8 h, the infected areas microdissected and prepared for confocal microscopy. Nuclear morphology allowed identification of numerous cell types in the vasculature surrounding the infected tubule. Flat endothelial nuclei, were observed in the vessel wall (Fig. 5A, arrow). The majority of intravascular cells appeared to have large spherical nuclei, however, a few neutrophils were identifiable by their typical segmented nuclear shape (Fig. 5B). Whether these neutrophils are located in the vessel or are in the process of extravasating across the endothelium is unclear. Figure 5C shows a deeper confocal plane from Fig. 5A, where a neutrophil is identified within the tubular lumen having crossed both the endothelial and epithelial barriers. In multiphoton images, black voids as in Fig. 5D, were often observed within the tubules. These voids correlate well to the neutrophil in Fig. 5C, and demonstrate that neutrophil migration across the epithelium occurs 4–5 h post microinjection of bacteria. Specific adhesion molecules are required for neutrophil extravasation; intercellular adhesion molecule 1 (ICAM-1) is one of these molecules and specific antibody staining confirmed its expression on activated endothelium in the vicinity of the colonized tubule (red in Fig. 5E).

Prokaryotic and eukaryotic gene expression in vivo

To generate molecular details of the visualized processes, the infected nephron was microdissected after 8 h of imaging and the total RNA extracted. Gene expression was analysed using reverse transcription polymerase chain reaction (RT-PCR) (Fig. 5F). Microdissection reduced the dilution factor of the bacterial RNA and the technique allowed analysis of both prokaryotic and eukaryotic gene expression. 16S rRNA expression confirmed the presence of bacteria in the infected sample and GAPDH established the integrity of eukaryotic RNA. Bacterial infection triggered cells in the mucosal lining to directly or indirectly upregulate expression of the chemoattractant CINC-1 (homologue to human IL-8), and the presence of CD45 validated our findings of leukocyte recruitment. CINC-1 signalling was accompanied by an upregulation of the integrin lymphocyte function-associated antigen-1 (LFA-1), an important factor in the rolling and tethering of leukocytes to the endothelium. Upregulation of ICAM-1 was identified, giving molecular confirmation to the antibody data in Fig. 5E. TNF-α, a vasodilator that facilitates passage of immune cells from the vasculature to foci of infection, was also upregulated upon infection. Collectively, this showed that within 8 h of the first bacteria entering the tubule, major determinants triggering diapedesis and extravasation of neutrophils to the site of infection were expressed.

Renal morphological effects of wt UPEC and the virulence factor Hly in vivo

The exotoxin Hly is a known virulence factor in pyelonephritogenic *E. coli*. *In vitro*, high concentrations of Hly are cytolytic for erythrocytes and nucleated cells, while recent findings show that sublytic concentrations of Hly elicit intracellular Ca^{2+} signalling (Uhlen *et al*., 2000). *In vivo* expression of Hly was confirmed by RNA expression analysis at 8 h post injection (Fig. 5F). Despite expression of Hly, a four day retrograde infection model induced by the wild-type (wt) strain LT004 demonstrated no apparent histopathological differences as compared with the isogenic *hlyA*$^-$ strain LT005. Student's *t*-test (two-tailed, unpaired) also did not reveal any significant differences in the numbers of bacteria extracted from homogenized kidneys or urine samples (data not shown).

The micropuncture method provided an opportunity to study the effects of Hly on tissue pathology during the early hours of infection. The first images in each panel of Fig. 6 revealed normal blood flow when bacterial numbers were low. One hour later, bacteria had multiplied extensively in both animals, and severe effects on the vasculature were obvious in the wt-infected rat (LT004 + 1 h). This was followed by complete cessation of the blood flow and reduced delivery of the Hoechst stain (LT004 + 2.5 h and LT004 + 4 h). These rapid vascular effects were delayed by approximately 3 h in the *hlyA*$^-$ infected rats (LT005 + 4 h arrow). Black discs representing extravasated neutrophils were specifically found in the tubule lumens of wt-infected rats, supporting a role for Hly-induced pro-inflammatory signalling (Uhlen *et al*., 2000) during early stages of inflammation (Fig. 6 LT004 + 4 h vs. LT005 + 4 h).

Detached proximal tubule cells were observed as black discs lined with Cascade blue within the lumen of wt-infected tubules (Fig. 6 LT004 + 2.5 h, arrow) accompanying a loss of integrity of the epithelial lining (arrowhead). This may represent the cytolytic effect of Hly as in contrast, nothing similar was observed in *hlyA*$^-$ infected rats (Fig. 6 LT005).

Discussion

Cell culture studies have been instrumental in the development of the infection biology field over the last 20 years.

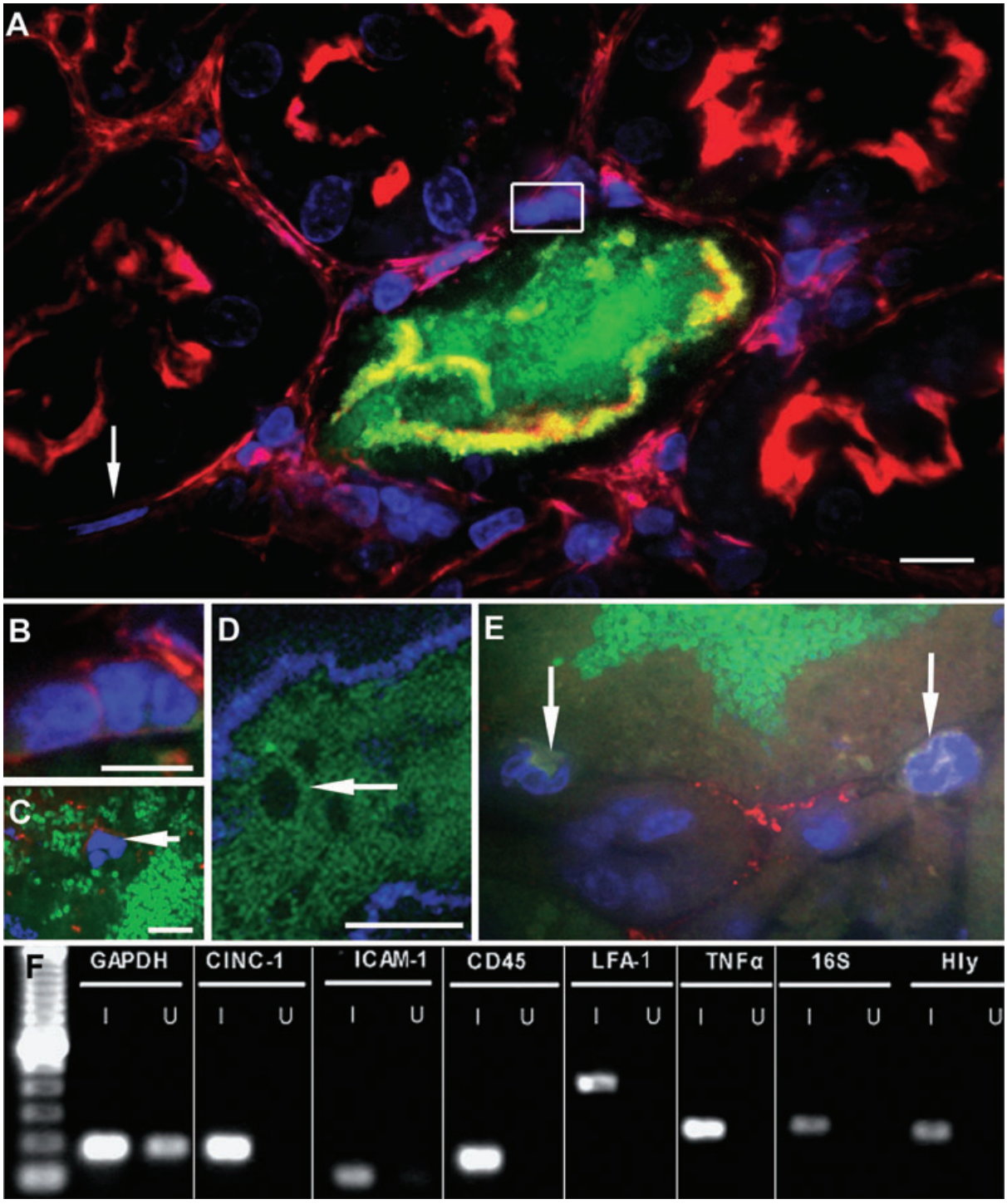

Fig. 5. Tissue remodelling 8 h after bacterial injection.
A. Microdissected foci of infection analysed *ex vivo* by confocal microscopy 8 h post injection. Bacteria are detected by GFP$^+$ (green), actin-rich structures by TRITC-phalloidin (red), cell nuclei by Hoechst (blue) and 10 kDa labelled dextran (pseudo-coloured yellow) outlines the injected tubule. Arrow indicates endothelial cell nucleus. Scale bar represents 10 μm.
B. Higher magnification of the boxed area in A reveals distinct neutrophils. Scale bar represents 5 μm.
C. Neutrophil (arrow) in the bacteria-filled tubular lumen. Scale bar represents 10 μm.
D. Multiphoton microscopy showing a black silhouette (arrow) in the tubular lumen that correlates with the neutrophils in (C). Scale bar represents 30 μm.
E. Endothelial ICAM–1 expression around an infected tubule (red). Arrows indicates neutrophils. Scale bar represents 10 μm.
F. RT-PCR analysis of kidneys 8 h post injection (I) or uninfected (U).

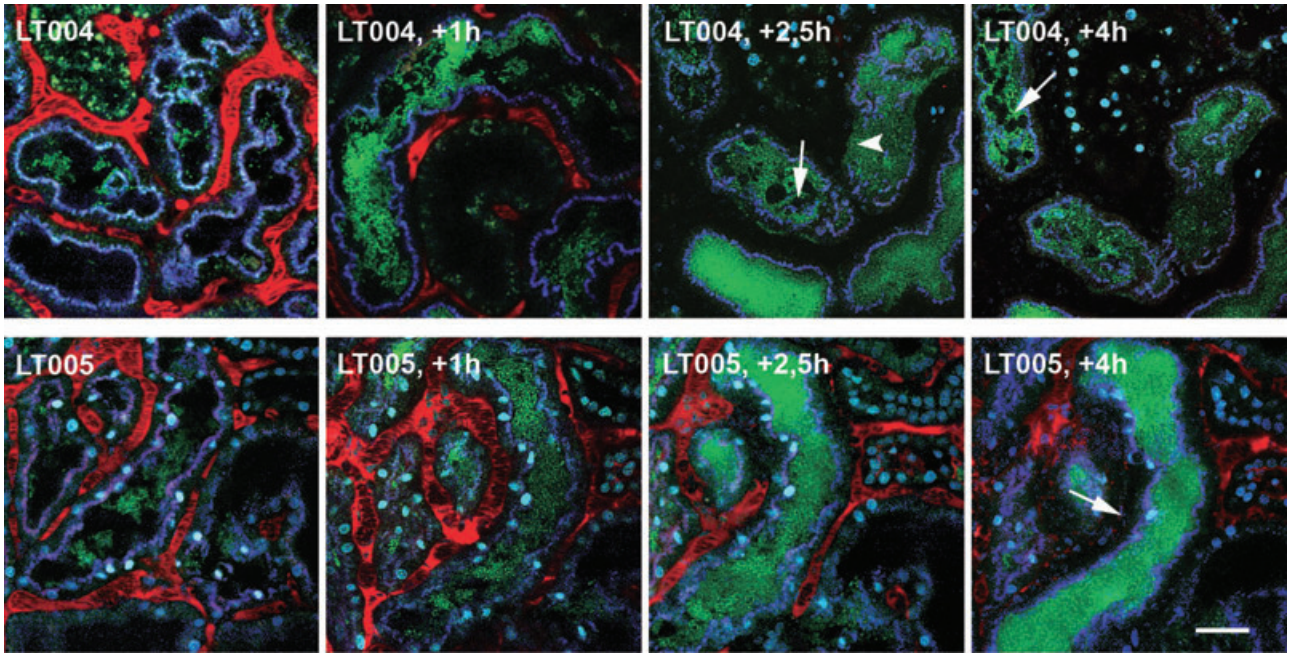

Fig. 6. Role of Hly in initiation of the immune response *in vivo*. Repeated multiphoton imaging after intratubular microinjection of either LT004 (Hly^+, upper panel) or LT005 (Hly^-, lower panel). Injected proximal tubules are outlined with labelled 10 kDa dextran (blue), blood flow are visualized by labelled 500 kDa dextran (red) and bacteria detected by GFP^+ (green). Representative images depict the progression of infection 1 h, 2.5 h and 4 h after bacterial colonization of injected nephrons. Arrow in LT004 + 2.5 h indicate detached proximal tubule cell and arrowhead specifies disrupted epithelial lining. Arrow in LT004 + 4 h indicates extravasated neutrophil, while arrow in LT005 + 4 h shows compromised blood flow. Scale bar represents 30 μm.

More recently it has been shown that local injuries such as bacterial infections, elicit a co-ordinated tissue response within the host, which is impossible to study in the simplified cell culture model. The multiphoton microscopy technique we employ in the present study, has been described as the last step in reverse-reductionism, taking the model system from cell culture back to the living animal (Molitoris and Sandoval, 2005). By adapting this technology to infection biology studies, a new field of research embracing microbe-induced organ and tissue specific cell communication is opened.

We show that a single-copy of the genetically enhanced GFP^+ variant, where altered protein folding results in improved fluorophore intensity (Scholz *et al*., 2000), is sufficient for bacterial detection *in vivo*. The $P_{LtetO-1}$ promoter is shown to be suitable to ensure GFP^+ expression from bacteria multiplying inside the tissue. The absence of the gene encoding the *tet* repressor altered $P_{LtetO-1}$ from an inducible to a constitutively active promoter, thus eliminating the need for induction *in vivo*. In contrast, the commonly used P_{rpsM} promoter, normally associated with expression of ribosomal proteins, was found to be inappropriate, with only a fraction of tissue-localized bacteria able to express GFP^+ under the control of this promoter (data not shown). Bacteria are extremely efficient at adapting their physiology to the changing growth environments encountered during the course of infection. This occurs primarily by changing their ribosomal content (Neidhardt *et al*., 1990), a possible reason for differential expression under the P_{rpsM} promoter.

Micropuncture is a well-established technique for studying renal function (Tanner *et al*., 2005) and we exploited this method to deliver bacteria directly into the lumen of proximal tubules. This allowed us to dictate both the spatial and temporal parameters and infection kinetics could accordingly be studied with a defined time scale. This is in contrast to the retrograde pyelonephritis model where random numbers of bacteria ascend from the bladder at random time points into random nephrons. Our technique avoided many of the problems related to spatial and temporal specificity as well as differentiation between involvement of bladder and kidney tissue, a problem when measuring infection markers in voided urine.

Onset of the inflammatory response is considered to be the major cause of tissue injury in pyelonephritis (Bille and Glauser, 1982). The inflammatory cytokine profile suggests that the response is confined to the kidney, not involving extra-renal, lymphoid organs (Rugo *et al*., 1992; Kabore *et al*., 1999). We visualized for the first time the kinetics of neutrophil recruitment in real-time. Neutrophils started to appear at the infection site as early as 3–4 h post injection, and by 8 h, they con-

stituted approximately 20–40% of nucleated cells present in the vasculature. Not until 22 h post injection were neutrophils, generally considered as the foremost inflammatory cell, the predominant cell type at the infection foci. Although this work confirmed previous studies (Shimamura, 1981; Haraoka *et al*., 1999) demonstrating the importance of neutrophils in the antibacterial defence of the urinary tract, we also detected other nucleated cells recruited at this very early time point to the site of infection. Future experiments will reveal the nature of these nucleated cells.

One parameter contributing to the development of necrotic tissue is disruption of the vasculature. The kidney is a highly vascularized organ and the close relationship between epithelial and endothelial barriers makes pyelonephritis an excellent model for studying vascular effects of bacterial infection. Our study reveals that, within hours, ischaemia occurred in capillaries surrounding the infected tubule. This may result in part from recruitment of activated leukocytes. As they move slowly through the capillary microvasculature leukocytes contribute to congestion and vessel occlusion. Leukocytes traversing the endothelium can disrupt intercellular connections, and the release of reactive oxygen species from activated leukocytes may exacerbate damage to the vessel and surrounding tissue (Marcus *et al*., 1997; Gute *et al*., 1998). The immune cell recruitment may result from bacteria-induced epithelial signalling, with proximal tubule cells being known producers of a variety of signalling molecules in response to bacterial exposure (Kabore *et al*., 1999; Uhlen *et al*., 2000; Laestadius *et al*., 2003). This signalling may explain the localization of vasculature disruption to the infected nephron, with adjacent, non-infected nephrons appearing normal.

The ability to identify the microinjected sites in exteriorized kidneys provided the possibility to microdissect infected nephrons to study the molecular details of tissue signalling on either protein or gene expression level. Bacterial RNA could be isolated along with eukaryotic RNA, allowing prokaryotic gene expression analysis. This resulted in confirmation of Hly expression *in vivo* for the first time. A role for this virulence factor in augmenting the inflammatory response during the first hours of the infection process was also identified. The level of Hly in the tissue is likely to be low at this early phase of infection. Low concentrations of Hly have been shown to activate a Ca^{2+}-dependent signal-transduction pathway in renal epithelial cells, leading to production of pro-inflammatory cytokines (Uhlen *et al*., 2000), suggesting a role for toxin-induced signalling in recruitment and transmigration of neutrophils. At high concentration the pore-forming Hly has been shown to be a cytolytic toxin and in our studies the massive multiplication of bacteria occurring with the first hours of infection may enable local concentrations of hly to reach cytolytic levels, causing disruption of the integrity of epithelial and endothelial barriers.

To orchestrate a co-ordinated tissue response to bacterial infection, the integration and transduction of multiple signals is required to produce a suitable inflammatory response. The restricted availability of appropriate techniques has hampered previous work in this area. We hope that the methods described herein can be utilized to study tissue responses to a variety of bacterial pathogens and their virulence factors, where the spatio-temporal resolution is key to understand the inflammatory processes.

Experimental procedures

Bacterial strains and plasmids

Bacterial strains and oligonucleotide sequences used in this study are listed in Table 1. Genetic manipulations were performed in the pyelonephritogenic *E. coli* strain CFT073 (O6:K2:H1, American Type Culture Collection no. 700928, GeneBank Accession no. AE014075) (Mobley *et al*., 1990; Welch *et al*., 2002). Bacteria were cultivated in Luria–Bertani medium at 37°C in the presence of ampicillin (Amp, 100 μg ml^{-1}), chloramphenicol (Cm, 20 μg ml^{-1}) and kanamycin (Km, 50 μg ml^{-1}) when indicated.

A Hly-negative isogenic isolate of CFT073 was constructed by a one-step allelic knock-out method (Datsenko and Wanner, 2000). The kanamycin resistance cassette from plasmid pKD4 was inserted into the *hlyA* gene, deleting 1840 bp between nt 3419219-3421058. Primers P1hly and P2hly include homology to priming sites 1 and 2 on pKD4 along with a 39 bp sequence homologous to the *hlyA* gene. PCR products were digested with *Dnp*1 (Sigma, Germany) and purified. The resulting 16 kb product was introduced into CFT073 harbouring the λ Red recombinase expression plasmid pKD46. Deletion of *hlyA* in the resulting strain LT002 was confirmed by sequence analysis (ABI3100, Applied Biosystems) and loss of haemolytic activity was controlled as described (Bhakdi *et al*., 1986).

GFP-producing bacteria were constructed by site-specific integration of the gene encoding enhanced green fluorescent protein (*gfp+)* onto the chromosome (Hautefort *et al*., 2003). The tetracycline promoter $P_{LtetO-1}$ was used in the absence of the Tet repressor, resulting in constitutive activation of the promoter (pPROTet.E 6xHN vector, BD Bioscience, USA). The promoter sequence was amplified using primers Ptet_R1 and Ptet_F1. The resulting PCR product and the *gfp*$^+$-*cm*^{r} containing plasmid pZEP08 (Hautefort *et al*., 2003) were digested with XbaI and SmaI (Sigma, Germany), purified and ligated, resulting in the plasmid pKM001, templates for PCR amplification of sequences for site-specific recombination into the *cobS* gene sequence. PCR amplification of plasmids pKM001 ($P_{LtetO-1}$-*gfp*$^+$-*cm*^{r}) and pZEP07 (promoterless *gfp*$^+$-*cm*^{r}) (Hautefort *et al*., 2003) were performed with primers P1cob and P2cob containing a 5′ 40 nt region fully homologous to the *cobS* locus, at 44 min on the CFT073 chromosome. The remaining 21–23 nt sequences contain binding sites to the *gfp*$^+$-*cm*^{r}-containing plasmids. Chromosomal recombination of PCR products was achieved using λ

Red recombination (Datsenko and Wanner, 2000), deleting 1143 bp (positions 2319458-2320600). PCR fragments from pKM001 were also introduced into strain LT002, creating a *hlyA*-negative GFP-expressing isolate of CFT073. Chloramphenicol-resistant *E. coli* transformants were sequenced (ABI 3100 sequencer, Applied Biosystems), and named as in Table 1. GFP-expressing bacteria *in vitro* and *in vivo* using *E. coli* OK K13 monovalent rabbit antiserum (Statens Serum Institut, Denmark) and GtαRbCy3 (Jackson Immunoresearch Laboratory, USA). Expression of GFP^+ did not alter bacterial physiology as measured by bacterial growth rates and haemolysis assays (data not shown).

Retrograde infection model of acute pyelonephritis

Bladders of isofluran-anaesthesized, 214 ± 10 g ($n = 49$ in total for retrograde infections) female Sprague-Dawley rats (B and K Universal AB) were catheterized and 10^8 cfu of *E. coli* strains LT003 ($n = 10$), LT004 ($n = 20$), or LT005 ($n = 14$) in 1 ml of PBS, or PBS alone ($n = 5$), were slowly infused. Four days after infection, rats were prepared for live multiphoton microscope (as described below), and/or sacrificed to provide material for kidney and urine bacterial counts, RNA extraction or immunohistochemistry. A minimum of five rats from each infection group was studied by each individual technique, and representative images from each set of experiments were selected for display in Figs 1B and 2. All animal studies have been approved by Stockholms Norra Djurförsöksetiska Nämnd and/or the Institutional Animal Care and Use Committee and were performed in accordance with the National Institutes of Health's *Guide for the Care and Use of Laboratory Animals*.

Intratubular micropuncture

LT004 and LT005 were cultivated to OD_{600} 0.6 and concentrated to 10^9 cfu ml^{-1} in PBS containing 1 mg ml^{-1} Fast Green FCF (Fisher, Fair Lawn, NJ, USA) and 0.2 mg ml^{-1} Cascade blue-conjugated 10 kDa dextran. The suspension was aspirated into sharpened micropipettes (tip diameter 7–8 μm) filled with heavy mineral oil. Male Sprague-Dawley rats, 252 ± 32 g ($n = 10$), were anaesthetized by intraperitoneal injection of 40–50 mg kg^{-1} sodium pentobarbital. On a heated animal board, the left kidney was exposed via a subcostal flank incision and supported in a cup. Under stereoscopic microscope observation (96×), using a Leitz micromanipulator and mercury-levelling bulb, the bacterial suspension was injected into two to three proximal tubules in each rat for 10 min ($n = 7$ for LT004 and $n = 4$ for LT005). The rate of infusion averaged 49 ± 23 nl min^{-1} ($n = 7$), which corresponded to delivery of ~5×10^5 cfu. As controls, five tubules were injected with sterile PBS. Experiments were repeated on different days with freshly prepared bacterial cultures. To aid in localization of injection sites, a nearby proximal tubule was filled with Sudan black-stained castor oil.

Multiphoton microscopy

All multiphoton imaging was conducted using the previously optimized and described set-up (Dunn *et al*., 2002). The excitation wavelength was 810 nm and neutral density filters set to 25–40%. Image stacks were collected by 1 μm optical steps into the tissue to a maximal depth of 100 μm. Time series were from images collected every second at the same optical plane for ~40 s.

Rats with exteriorized kidneys were transferred from sodium pentobarbital to halothane/oxygen anaesthesia, allowing fine-tuning and recovery. A venous access line was inserted into the femoral vein for dye infusion; rhodamine-tagged 500 kDa dextran (~2.5 mg per 400 μl of 0.9% saline, Molecular Probes, OR) for visualization of blood flow or Hoechst 33342 (~600 μg per 400 μl of 0.9% saline, Molecular Probes, OR) for nuclear staining. Rats were positioned on the microscope stage with the exposed kidney placed in a 50-mm-diameter coverslip-bottomed cell culture dish (Warner Instruments, CT, USA) and bathed in isotonic saline. A heating pad was placed directly over the rat and rectal temperature and arterial blood pressure were monitored. Representative images and movies from rats injected with the various stimuli are displayed in Figs 2–6.

Image processing

Images and data-volumes were processed using Image J (U. S. National Institutes of Health, MD, USA, http://rsb.info.nih.gov/ij/), Metamorph Image Processing Software (Universal Imaging-Molecular Devices, PA, USA) and Adobe Photoshop (Adobe, CA, USA). Three-dimensional projections were produced using Voxx volume-rendering software (Clendenon *et al*., 2002) and time-lapse movies were made using Image J.

Immunohistochemistry

Ten μm thick tissue slices were treated as described (Richter-Dahlfors *et al*., 1997) and analysed by confocal microscopy. Antibodies used were MsαRt-CD18, MsαRt-CD54 (ICAM-1) (BD Pharmingen, Sweden) and DkαMs-Cy3 (Jackson, USA) in addition to TRITC-conjugated phalloidin (Sigma, Germany) and Hoechst 33342 (Molecular Probes, OR).

RT-PCR

Total RNA was extracted by TRIzol (Invitrogen, CA, USA), purified and converted to cDNA. PCR was performed using primers for GAPDH, CINC-1, ICAM-1, LFA-1, CD45, TNF-α, 16S rRNA and HlyA and a thermocycling program of 94°C 2 min, 94°C 30 s, 60°C 30 s, 74°C 1 min.

Acknowledgements

We thank J. Hinton (Institute of Food Research, Norwich, UK) for providing plasmids prior to publication, E. Flaberg and L. Szekely (Microbiology and Tumor Biology Center, Karolinska Institutet) for confocal microscopy advice and F. Torstensson (Smedby digital) for providing the cartoon in Fig. 2A. The work was supported by grants from the Royal Swedish Academy of Sciences, the Swedish Foundation for Strategic Research, the Swedish Research Council (A.R.D.), Svenska Läkarsällskapet, Erik och Edith Fernströms Stiftelse (L.E.M.), National Institutes of Health Grants P01 DK-53465 and DK069408 (B.A.M.). Live imaging data were generated at The Indiana Center for Biological

Microscopy. No financial conflicts of interest apply to any of the authors.

References

Bhakdi, S., Mackman, N., Nicaud, J.M., and Holland, I.B. (1986) *Escherichia coli* hemolysin may damage target cell membranes by generating transmembrane pores. *Infect Immun* **52:** 63–69.

Bille, J., and Glauser, M.P. (1982) Protection against chronic pyelonephritis in rats by suppression of acute suppuration: effect of colchicine and neutropenia. *J Infect Dis* **146:** 220–226.

Brown, E.B., Campbell, R.B., Tsuzuki, Y., Xu, L., Carmeliet, P., Fukumura, D., and Jain, R.K. (2001) *In vivo* measurement of gene expression, angiogenesis and physiological function in tumors using multiphoton laser scanning microscopy. *Nat Med* **7:** 864–868.

Clendenon, J.L., Phillips, C.L., Sandoval, R.M., Fang, S., and Dunn, K.W. (2002) Voxx: a PC-based, near real-time volume rendering system for biological microscopy. *Am J Physiol Cell Physiol* **282:** C213–C218.

Datsenko, K.A., and Wanner, B.L. (2000) One-step inactivation of chromosomal genes in *Escherichia coli* K-12 using PCR products. *Proc Natl Acad Sci USA* **97:** 6640–6645.

Dunn, K.W., Sandoval, R.M., Kelly, K.J., Dagher, P.C., Tanner, G.A., Atkinson, S.J., *et al.* (2002) Functional studies of the kidney of living animals using multicolor two-photon microscopy. *Am J Physiol Cell Physiol* **283:** C905–C916.

Dunn, K.W., Sandoval, R.M., and Molitoris, B.A. (2003) Intravital imaging of the kidney using multiparameter multiphoton microscopy. *Nephron Exp Nephrol* **94:** e7–11.

Glauser, M.P., Lyons, J.M., and Braude, A.I. (1978) Prevention of chronic experimental pyelonephritis by suppression of acute suppuration. *J Clin Invest* **61:** 403–407.

Gute, D.C., Ishida, T., Yarimizu, K., and Korthuis, R.J. (1998) Inflammatory responses to ischemia and reperfusion in skeletal muscle. *Mol Cell Biochem* **179:** 169–187.

Haraoka, M., Hang, L., Frendeus, B., Godaly, G., Burdick, M., Strieter, R., and Svanborg, C. (1999) Neutrophil recruitment and resistance to urinary tract infection. *J Infect Dis* **180:** 1220–1229.

Hautefort, I., Proenca, M.J., and Hinton, J.C. (2003) Single-copy green fluorescent protein gene fusions allow accurate measurement of Salmonella gene expression *in vitro* and during infection of mammalian cells. *Appl Environ Microbiol* **69:** 7480–7491.

Heptinstall, R.H., and Hill, G.S. (1983) *Pathology of the Kidney*. Boston, MA: Little, Brown and Company.

Jahnukainen, T., Chen, M., and Celsi, G. (2005) Mechanisms of renal damage owing to infection. *Pediatr Nephrol* **20:** 1043–1053.

Kabore, A.F., Simard, M., and Bergeron, M.G. (1999) Local production of inflammatory mediators in an experimental model of acute obstructive pyelonephritis. *J Infect Dis* **179:** 1162–1172.

Karin, M., and Greten, F.R. (2005) NF-kappaB: linking inflammation and immunity to cancer development and progression. *Nat Rev Immunol* **5:** 749–759.

Laestadius, A., Soderblom, T., Aperia, A., and Richter-Dahlfors, A. (2003) Developmental aspects of *Escherichia coli*-induced innate responses in rat renal epithelial cells. *Pediatr Res* **54:** 536–541.

Lax, A.J., and Thomas, W. (2002) How bacteria could cause cancer: one step at a time. *Trends Microbiol* **10:** 293–299.

Marcus, B.C., Hynes, K.L., and Gewertz, B.L. (1997) Loss of endothelial barrier function requires neutrophil adhesion. *Surgery* **122:** 420–427.

Mobley, H.L., Green, D.M., Trifillis, A.L., Johnson, D.E., Chippendale, G.R., Lockatell, C.V., *et al.* (1990) Pyelonephritogenic *Escherichia coli* and killing of cultured human renal proximal tubular epithelial cells: role of hemolysin in some strains. *Infect Immun* **58:** 1281–1289.

Molitoris, B.A., and Sandoval, R.M. (2005) Intravital multiphoton microscopy of dynamic renal processes. *Am J Physiol Renal Physiol* **288:** F1084–F1089.

Neidhardt, F.C., Ingraham, J.L., and Schaechter, M. (1990) *Physiology of the Bacterial Cell: A Molecular Approach*. Sunderland, MA: Sinauer Associates.

Pass, D., and Freeth, G. (1993) The rat. *ANZCCART News* **6:** 1–4.

Philpott, D.J., Girardin, S.E., and Sansonetti, P.J. (2001) Innate immune responses of epithelial cells following infection with bacterial pathogens. *Curr Opin Immunol* **13:** 410–416.

Richter-Dahlfors, A., Buchan, A.M., and Finlay, B.B. (1997) Murine salmonellosis studied by confocal microscopy: *Salmonella typhimurium* resides intracellularly inside macrophages and exerts a cytotoxic effect on phagocytes *in vivo*. *J Exp Med* **186:** 569–580.

Rugo, H.S., O'Hanley, P., Bishop, A.G., Pearce, M.K., Abrams, J.S., Howard, M., and O'Garra, A. (1992) Local cytokine production in a murine model of *Escherichia coli* pyelonephritis. *J Clin Invest* **89:** 1032–1039.

Scholz, O., Thiel, A., Hillen, W., and Niederweis, M. (2000) Quantitative analysis of gene expression with an improved green fluorescent protein. p6. *Eur J Biochem* **267:** 1565–1570.

Shimamura, T. (1981) Mechanisms of renal tissue destruction in an experimental acute pyelonephritis. *Exp Mol Pathol* **34:** 34–42.

Squirrell, J.M., Wokosin, D.L., White, J.G., and Bavister, B.D. (1999) Long-term two-photon fluorescence imaging of mammalian embryos without compromising viability. *Nat Biotechnol* **17:** 763–767.

Tanner, G.A., Sandoval, R.M., Molitoris, B.A., Bamburg, J.R., and Ashworth, S.L. (2005) Micropuncture gene delivery and intravital two-photon visualization of protein expression in rat kidney. *Am J Physiol Renal Physiol* **289:** F638–F643.

Uhlen, P., Laestadius, A., Jahnukainen, T., Soderblom, T., Backhed, F., Celsi, G., *et al.* (2000) Alpha-haemolysin of uropathogenic *E. coli* induces Ca2+ oscillations in renal epithelial cells. *Nature* **405:** 694–697.

Welch, R.A., Burland, V., Plunkett, G., 3rd, Redford, P., Roesch, P., Rasko, D., *et al.* (2002) Extensive mosaic structure revealed by the complete genome sequence of

uropathogenic *Escherichia coli*. *Proc Natl Acad Sci USA* **99:** 17020–17024.

Supplementary material

The following supplementary material is available for this article online:

Movie S1. Normal tissue morphology and blood flow in a PBS-control rat imaged by multiphoton microscopy. Fluorescent 500 kDa dextran labels blood flow (red), cell nuclei are labelled with Hoechst stain (blue) and proximal tubules are identified by dull green auto-fluorescence. Animation of a series of images collected every second on the same focal-plane during a 40 s time period, from which one frame is shown as Fig. 2B.

Movie S2. Disrupted tissue morphology in an LT004 infected rat kidney imaged by multiphoton microscopy. Fluorescent 500 kDa dextran labels blood flow (red), cell nuclei are labelled with Hoechst stain (blue), proximal tubules are identified by dull green auto-fluorescence and bacteria detected by GFP^+ (green). Animation of the 3D-projection presented in Fig. 2D of an 18-μm-thick tissue volume of images collected by 1 μm steps.

This material is available as part of the online article from http://www.blackwell-synergy.com

